ACS OMEGA

Open Access

http://pubs.acs.org/journal/acsodf

Article

Electrochemical Epoxidation of Propylene to Propylene Oxide via Halogen-Mediated Systems

Jiangjiang Wang, Gangfeng Wu, Guanghui Feng, Guihua Li, Yiheng Wei, Shoujie Li, Jianing Mao, Xiaohu Liu, Aohui Chen, Yanfang Song, Xiao Dong,* Wei Wei,* and Wei Chen*

Cite This: *ACS Omega* 2023, 8, 46569−46576

Read Online

ACCESS | Metrics & More | Article Recommendations | Supporting Information

ABSTRACT: As one of the most important derivatives of propylene, the production of propylene oxide (PO) is severely restricted. The traditional chlorohydrin process is being eliminated due to environmental concerns, while processes such as Halcon and hydrogen peroxide epoxidation are limited by cost and efficiency, making it difficult to meet market demand. Therefore, achieving PO production through clean and efficient technologies has received extensive attention, and halogen-mediated electrochemical epoxidation of alkene is considered to be a desirable technology for the production of alkylene oxide. In this work, we used electrochemical methods to synthesize PO in halogen-mediated systems based on a RuO_2-loaded Ti (RuO_2/Ti) anode and screened out two potential mediated systems of chlorine (Cl) and bromine (Br) for the electrosynthesis of PO. At a current density of 100 mA·cm^{-2}, both Cl- and Br-mediated systems delivered PO Faradaic efficiencies of more than 80%. In particular, the Br-mediated system obtained PO Faradaic efficiencies of more than 90% at lower potentials (≤1.5 V vs RHE) with better electrode structure durability. Furthermore, detailed product distribution investigations and DFT calculations suggested hypohalous acid molecules as key reaction intermediates in both Cl- and Br-mediated systems. This work presents a green and efficient PO production route with halogen-mediated electrochemical epoxidation of propylene driven by renewable electricity, exhibiting promising potential to replace the traditional chlorohydrin process.

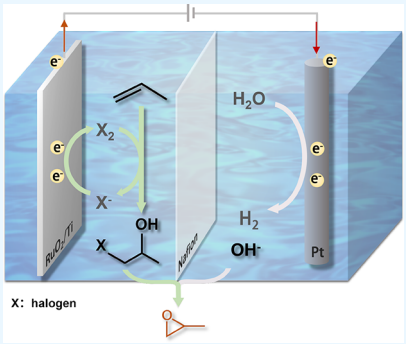

1. INTRODUCTION

Propylene oxide (PO) is an important raw material in the fine chemical production process and is widely used in the production of polyurethane and propylene glycol. The total PO production has increased year by year and exceeded 10 million tons. Common industrial methods for PO production include the chlorohydrin process,[1] the Halcon process,[2,3] and the hydrogen peroxide process.[4] The chlorohydrin process requires a large amount of chlorine gas, which is harmful to the environment and generates a large amount of solid waste ($CaCl_2$). The Halcon process has limited economic benefits due to the insufficient market demand for its coproducts (either styrene or *tert*-butyl alcohol), while the hydrogen peroxide process is restricted by the high cost of H_2O_2.[5,6] Thus, it is urgent to develop an environmentally friendly, low-cost, and efficient process to achieve PO production.

Since the conversion of propylene to PO is an oxidation reaction, there is potential to achieve this process through the electrochemical epoxidation on the anode, offering advantages of using clean electrical energy for PO production. Furthermore, coupling this process with cathodic reactions such as hydrogen evolution or carbon dioxide electroreduction provides more promise for maximizing its economic value.[7]

Typically, the electrochemical epoxidation of propylene is achieved in two ways: one is the direct oxidation of propylene on the anode with active oxygen species; the other is the indirect oxidation of propylene using intermediate species with moderate oxidizing properties such as halogens in their oxidation state formed on the anode. Unfortunately, the direct oxidation of propylene to PO through an electrochemical method is currently severely restricted by the poor product selectivity and efficiency.[8,9] Hence, halogen-mediated electrochemical methods have received more and more attention.[10] At present, chlorine-mediated electrochemical epoxidation of olefins such as ethylene and styrene is receiving extensive interest.[11,12] Compared with the chlorohydrin process in industry, the halogen-mediated electrochemical epoxidation method uses halogen as a medium to continuously circulate in the system to avoid large amounts of waste residue emissions and to improve economy.[1] In addition, compared with the thermally mediated epoxidation using oxygen as the oxygen source with a reaction temperature of around 200 °C, the electrochemical epoxidation using H_2O as the oxygen source at

Received: July 28, 2023
Revised: October 18, 2023
Accepted: November 21, 2023
Published: December 1, 2023

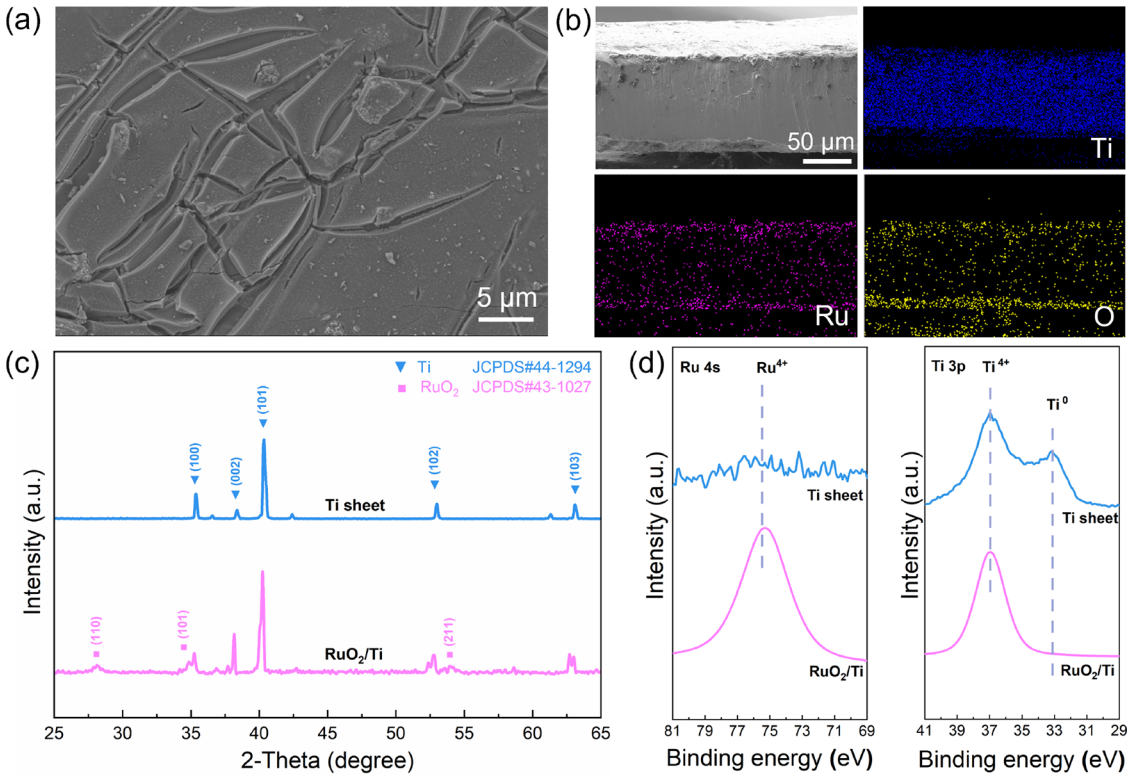

Figure 1. (a) Surface morphology as well as (b) cross-sectional morphology and elemental distribution of RuO_2/Ti. (c) XRD patterns as well as (d) Ru 4s and Ti 3p XPS curves of RuO_2/Ti and the Ti sheet support.

ambient conditions is more operable and safer and could achieve higher selectivity and yields.[13,14] However, among all halogen systems, the chlorine-mediated system has a relatively higher cell potential and energy loss due to the high standard potential of chlorine, which is also similar to that of the competitive oxygen evolution reaction (OER).[15]

Herein, we explored the potential of different halogen systems to mediate the electrochemical epoxidation of propylene, using titanium-supported ruthenium dioxide (RuO_2/Ti) as the anode, to obtain halogen-mediated systems with better propylene electrochemical epoxidation performance and efficiency. Additionally, we identified the reaction intermediate species by the experimental investigation of the product distribution in electrolytes with different halogen concentrations as well as density functional theory (DFT) calculations.

2. EXPERIMENTAL AND COMPUTATIONAL SECTION

2.1. Catalyst Synthesis. RuO_2 was loaded on a titanium sheet by a hot coating and sintering method. First, the titanium sheet was mechanically polished and ultrasonicated in deionized water and ethanol for 10 min. Pretreated titanium sheets were boiled in 15 wt % oxalic acid solution for 30 min. $RuCl_3{\cdot}xH_2O$ powder was dispersed into 1 M HCl aqueous solution at about 50 °C and configured as a coating solution with a mass fraction of about 30%. The titanium sheets were immersed into the coating solution for 30 s, dried at 80 °C, and then sintered at 500 °C for 2 h in air. The above coating steps were repeated 10 times out on the bench to obtain the RuO_2/Ti anode (Figure S1). IrO_2 and PdO coatings were prepared through a similar process, except that $RuCl_3{\cdot}xH_2O$ was replaced with $IrCl_3$ and $PdCl_2$.

2.2. Materials Characterization. XRD patterns of the RuO_2/Ti catalysts were obtained by X-ray diffraction (Rigaku Ultima IV) with Cu Kα radiation (λ = 1.54 Å) under 40 kV, 40 mA, and a scanning speed of $2°{\cdot}min^{-1}$. X-ray photoelectron spectroscopy (XPS) was measured by a Thermo K-Alpha XPS instrument with a monochromatic Al Kα source ($h\nu$ = 1486.6 eV) Quantum 2000 scanning ESCA microprobe under 12 kV and 4 mA. The surface morphologies and elemental distribution of the RuO_2/Ti catalysts were performed on a scanning electron microscope (SEM) (Zeiss SUPRA 55 SAPPHIRE) with energy-dispersive X-ray spectroscopy (EDS) with acceleration voltages of 6.0 and 15.0 kV, respectively.

2.3. Electrochemical Measurement. The electrochemically active surface area (ECSA) of each electrode was evaluated via the double-layer capacitance (C_{dl}), which was determined by the cyclic voltammetry (CV) measurements in 1 M KBr at the potential range from 0.70 to 0.80 V (vs RHE, reversible hydrogen electrode) and 1.30 to 1.40 V in 1 M KCl with different scan rates (20−100 $mV{\cdot}s^{-1}$). Linear sweep voltammetry (LSV) was conducted with a scan rate of 10 $mV{\cdot}s^{-1}$ in Ar-saturated 1 M KBr or KCl at the potential range from 0.80 to 2.50 V. The electrochemical impedance spectroscopy (EIS) measurements were tested at the open-circuit voltage, with the frequency range from 100 Hz to 200 kHz and a voltage amplitude of 10 mV.

Propylene epoxidation reaction (PER) measurements were evaluated through a three-electrode configuration in 1 M KCl/KBr/KI with the continuous feeding of propylene at ambient temperature and pressure using a two-compartment electrochemical H-type cell separated by a Nafion membrane (Figure S2). A KCl-saturated $Hg/HgCl_2$ electrode and a platinum wire electrode were used as the reference and counter electrode,

https://doi.org/10.1021/acsomega.3c05508
ACS Omega 2023, 8, 46569−46576

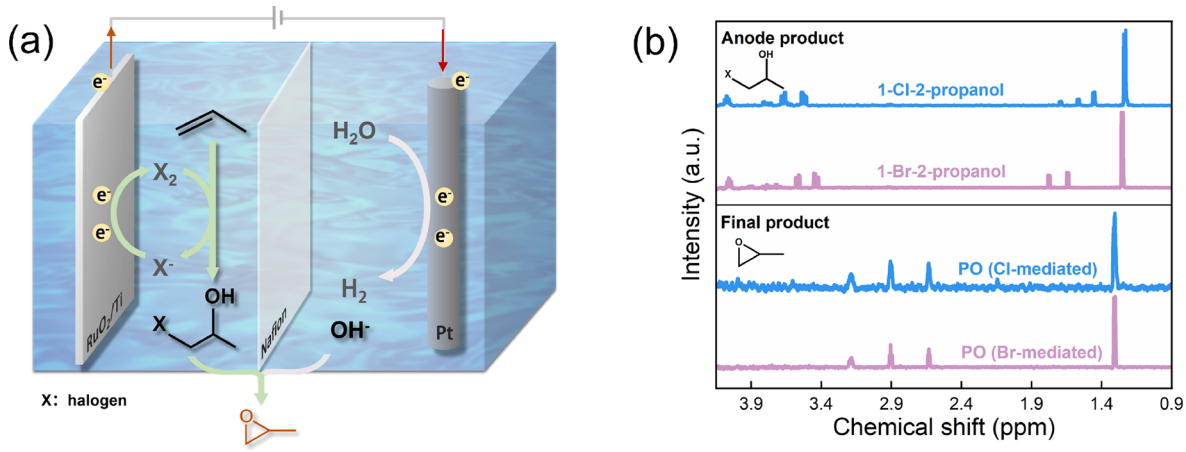

Figure 2. (a) Schematic diagram of the reaction process. (b) Product identification via the ^{1}H NMR spectra.

respectively. A CHI660e electrochemical workstation was used for current control and potential measurement. All the current densities in the manuscript and Supporting Information were geometrically normalized to the electrode area. All the applied potentials were recorded against the KCl-saturated $Hg/HgCl_2$ reference electrode and then converted to those versus the reversible hydrogen electrode (RHE) as E(vs RHE) = E(vs $Hg/HgCl_2$) + 0.2415 + 0.0591pH, where E(vs $Hg/HgCl_2$) (V) is the applied potential versus the $Hg/HgCl_2$ reference electrode and pH is the pondus hydrogenii value of the electrolyte solutions. Moreover, all applied potentials in the manuscript and Supporting Information are referred to vs RHE, unless otherwise stated. The error bars of electrocatalytic results were the standard deviation from at least three electrochemical tests for each condition.

2.4. Product Quantifications and Calculations. PO, chloropropanol, and bromopropanol were analyzed by a 500 MHz nuclear magnetic resonance (NMR) spectrometer (JNM-ECZ500R, JEOL, Japan). The PO product was quantified by the relative intensity of ^{1}H NMR at 1.3 ppm (Figure S3). The amount of halogen elements released from the liquid phase was determined by the concentration of hydroxide ions (eqs S4−S6), and the concentration of hydroxide ions was measured by a pH meter (PHBJ-260F, LeiCi Corp.) combined with a pH composite electrode (962244 LeiCi Corp.). Other active halogens in the liquid phase were quantified by the iodometric method (eqs S7 and S8). The Faradaic efficiency of each product was calculated by eq S9. More details can be found in the Supporting Information product quantification section.

2.5. Density Functional Theory (DFT) Calculations. Density functional theory (DFT) calculations were carried out using the Vienna ab initio simulation package (VASP) code with projected augmented wave (PAW) pseudopotentials.[16] The exchange−correlation contributions between electrons were calculated with the GGA functional proposed by Perdew−Burke−Ernzerhof (PBE).[17] The cutoff energy for the plane wave basis set was set to 400 eV. A vacuum of 20 Å in the z direction was employed in slab models to avoid the interactions between periodic images. The k-point sampling was obtained from the gamma scheme with a 1 × 1 × 1 mesh. The convergence criteria of energy and forces were set to 1×10^{-6} and 0.01 eV/Å, respectively. The vdW contributions were evaluated with the DFT-D3 method.[16,18] The reaction free energy for each elementary step is defined as $\Delta G = \Delta E + \Delta ZPE - T\Delta S$, where E is the electronic energy, ZPE is the zero-point energy, and S is the entropy. The ZPE can be calculated with ZPE = 1/2 $h\nu$ where h is the Plank constant and ν is the vibrational frequency of a normal mode. The implicit solvent model was used by VASPsol[19] to consider the effects of water. The free energy of each reaction step was balanced according to the reactants.

3. RESULTS AND DISCUSSION

3.1. Characterizations of the RuO_2/Ti Catalyst. The typical scanning electron microscopy image shows that the RuO_2 coating is tightly combined with the titanium substrate (Figure 1a), indicating that the oxidation of the substrate as well as the increase of charge transfer resistance during the anodic reaction would be avoided. Moreover, RuO_2 is distributed evenly on the Ti sheet surface, as demonstrated by the Ru and O elemental mappings via energy-dispersive X-ray spectroscopy (Figure 1b).

X-ray diffraction patterns of RuO_2/Ti in the range of 25−65° are shown in Figure 1c. The diffraction peaks corresponding to the spinel RuO_2 (110), (101), and (211) planes are observed (JCPDS no. 43-1027), along with three sharp characteristic (101), (002), and (200) peaks of metallic Ti (JCPDS no. 44-1294) from the Ti sheet. Moreover, the surface electronic states of the catalysts were analyzed by XPS. Due to the overlapping of Ru 3d and C 2p levels, as well as Ru 3p and Ti 2p levels, the XPS spectra of Ru 4s and Ti 3p were investigated instead to reveal the valence states of Ru and Ti in both samples, and the peaks of Ru^{4+} 4s at the binding energy of 75.9 eV indicates the presence of RuO_2 on the surface of the Ti support (Figure 1d).

3.2. Electrochemical Measurements and Performance. In the typical process of propylene electro-epoxidation (eqs S1−S3), propylene would first react with the halogen intermediate species in the anode region to generate the corresponding halohydrin, and then, these obtained halohydrins would be mixed with the cathode electrolyte, which contained the generated OH^- from the hydrogen evolution reaction on the cathode, to generate propylene oxide (Figure 2a). Preliminary tests showed that it is difficult for a F-mediated system to intervene in the epoxidation process because of its strong oxidizing trend to directly react with water.[20] When using KCl or KBr as the electrolyte, not only chloropropyl alcohol and bromopropyl alcohol were observed as the anode products, but also, PO was detected as the final

https://doi.org/10.1021/acsomega.3c05508
ACS Omega 2023, 8, 46569−46576

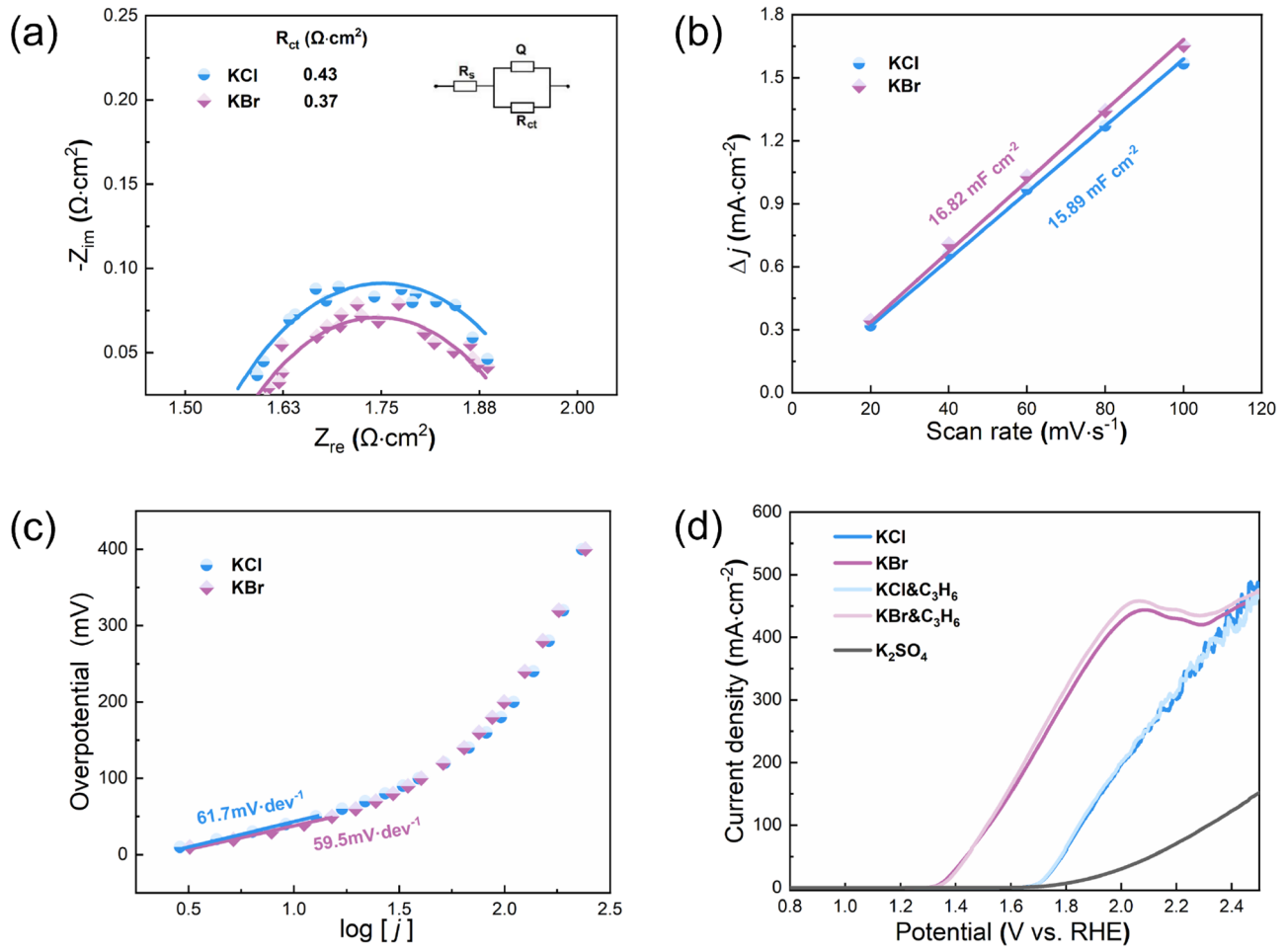

Figure 3. (a) EIS results, (b) ECSAs, (c) Tafel slopes, and (d) LSV curves of RuO_2/Ti in KCl and KBr.

product for both systems (Figure 2b and Figure S4a,b). In contrast, when using KI or K_2SO_4 as the electrolyte, no halopropanol or PO was observed as the products (Figure S4c). Thus, only both Cl and Br can intervene in the epoxidation process of propylene, and both Br- and Cl-mediated systems for PO electro-epoxidation were chosen for further investigations.

First, the electrochemical properties of the RuO_2/Ti electrode were investigated in Cl- and Br-mediated systems, respectively. It turned out that RuO_2/Ti exhibited similar electrochemical behaviors in both KCl and KBr. The charge transfer resistance of RuO_2/Ti in KCl is 0.43 Ω·cm², while that in KBr is 0.37 Ω·cm² (Figure 3a). As for the ECSAs of RuO_2/Ti (Figure S6), the values of C_{dl} (Figure 3b) in KCl and KBr are 16.82 and 15.89 mF·cm^{-2}, respectively, indicating the similar ECSAs of RuO_2/Ti. Meanwhile, the similar Tafel slopes indicate that both Cl- and Br-mediated systems have the same rate-determining steps in the process of sacrificing electrons on the catalyst surface (Figure 3c). The above evidence indicated that RuO_2/Ti showed similar electrochemical properties in both mediation systems.

Figure 3d shows LSV curves for the halogen precipitation reaction (HPR) and PER activity comparisons. It can be seen that the Br-mediated system has a lower onset potential of 1.36 V compared with that of 1.70 V for the Cl-mediated system. At the same time, the onset potential of 1.83 V for OER was tested in a potassium sulfate electrolyte. These results suggest that at the same overpotential, the Br-mediated system can alleviate the competing reaction of OER more effectively, thereby reducing the loss of energy efficiency from OER. Moreover, the shape distinctions of these LSV curves reflected the different diffusion characteristics of the oxidized halogen species in both systems. In the KCl system, the oxidation product is desorbed from the catalyst surface in its gas form, which would then escape easily from the electrode surface as bubbles. Therefore, the LSV curves especially at a large current density range of ≥200 mA·cm^{-2} became more and more fluctuant. In contrast, bromine produced during anodic oxidation would disperse into the electrolyte as a liquid and can freely diffuse on the electrode surface, leading to the smoothly extended LSV curves. In addition, the development and cracking of bubbles on the electrode surface usually accelerate the deterioration of the electrode structure.[21,22] Compared with the severe cracking of the coating in the Cl-mediated system, the electrode structure in the Br-mediated system is more stable under the same working conditions (Figure S7). However, when the current density was increased to 450 mA·cm^{-2}, the generated bromine accumulated on the electrode surface, inhibiting the advantageous Br-mediated PER kinetics and leading to the significantly increased potentials. No such phenomenon was observed in the Cl-mediated system at the whole current density range, indicating the essential differences for the reaction intermediates in both systems.

Then, the epoxidation performance of propylene was examined in both Cl- and Br-mediated systems with different

https://doi.org/10.1021/acsomega.3c05508
ACS Omega 2023, 8, 46569−46576

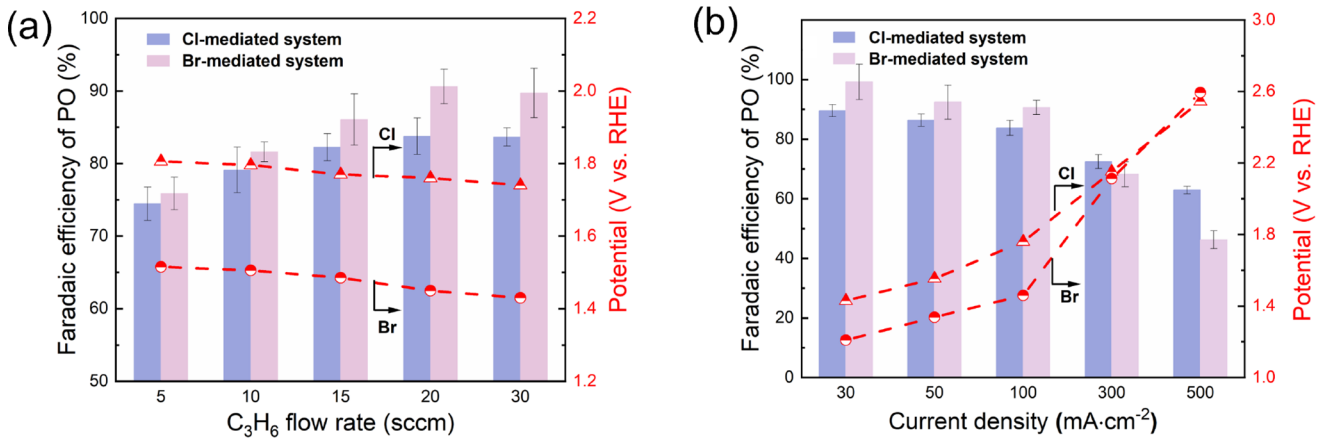

Figure 4. (a) FE_{PO} and applied potentials at different propylene flow rates and (b) current densities. The error bars correspond to the standard deviations of three independent measurements.

propylene flow rates and current densities at the constant electrolyte concentration of 1 M. As the flow rate of propylene increased from 5 to 30 sccm with the constant current density of 100 mA·cm^{-2}, the Faradaic efficiency of propylene oxide (FE_{PO}) increased from 74 to 80% in the Cl-mediated system with potentials of below 1.80 V. In contrary, the FE_{PO} exhibited a much larger increase (76 to 90%) in the Br-mediated system with potentials of not more than 1.50 V (Figure 4a). It is considered that chlorine has a relatively higher cell potential in the mediation process due to its higher thermodynamic potential and the anodic potential that is close to the oxidation potential of OER, leading to non-negligible energy loss in the chlorine-mediated system.[23] Simultaneously, the potential decreases (1.80 to 1.74 V in KCl and 1.51 to 1.42 V in KBr) while the FE_{PO} increases with the elevated flow rate of propylene, suggesting the enhanced utilization rate of the mediated halogen intermediate species, leading to promoted anodic process kinetics. This point is also confirmed by the LSV curves where the electrolyte saturated with propylene obtains higher current density than that the electrolyte without propylene at the same potentials (Figure 3d).

More detailed PER performances at different current densities were investigated at a propylene flow rate of 20 sccm, at which the FE_{PO} would achieve its maximum. Both mediation systems exhibited unique differences as the current density increased from 50 to 500 mA·cm^{-2} (Figure 4b). In the Cl-mediated system, with the increase of current density, FE_{PO} shows a continuous decay from 89.5 to 62.9%, as well as the rise of the potentials from 1.42 to 2.54 V with elevated OER. Meanwhile, in the Br-mediated system, FE_{PO} is close to 100% and is maintained at the level of more than 90% when the current density is below 100 mA·cm^{-2}. The stability of the electrode in different mediated systems was further tested under 100 mA cm^{-2} (Figure S10). The results show that the RuO_2/Ti electrode maintains good stability of the valence state and crystal structure with the potential around 1.70 V in the Cl-mediated system and 1.35 V in the Br-mediated system (Figure S9) and maintains stable FE_{PO} at the same time.

However, FE_{PO} decreases significantly to 68.2 and 46.2% when the current densities are further increased to 300 and 500 mA·cm^{-2}, with the significantly increased potentials from 1.20 to 2.59 V, losing its high PER energy efficiency advantages. Such a significant increase of the overpotential is due to the enrichment of Br_2 intermediate species in the liquid phase, hindering the further participation of intermediate species and slowing down the kinetics of the propylene oxidation process, which is consistent with the characteristics of the LSV curve (Figure 2d). The greatly elevated overpotential maintaining such a high current density would lead to a severely facilitated OER process, resulting in the dramatic reduction of FE_{PO}.

Compared with the traditional chlorohydrin process in industry, halogen-mediated electrochemical epoxidation can avoid the discharge of wastewater and residue through the circulation of the halogen in the system. The Br-mediated system in this work can reach a nearly 100% FE_{PO} at the current density of 30 mA cm^{-2}, and the halogen ions can be used as a circulation medium to mediate the production of PO with scarce wastewater and residue. In addition, compared with the thermally mediated epoxidation, which uses oxygen as the oxygen source at a reaction temperature of around 200 °C, the electrochemical epoxidation uses H_2O as the oxygen source at ambient conditions and is more operable and safer with higher selectivity and yields. The formation rate of PO, which is obtained based on FE and current density (eq S10), could achieve about 250 mg_{PO} h^{-1}·g_{cat}^{-1} with a PO selectivity of over 90% (Figure S10), which indicated the advantages of both operability and high efficiency compared with the thermally mediated processes (Table S1).

To further explore the applicability of the halogen-mediated electrochemical method, different electrode materials, Ti-supported IrO_2 (IrO_2/Ti) and Ti-supported PdO (PdO/Ti), were used for propylene epoxidation tests (Figures S11 and S12). The results show that IrO_2/Ti achieves good performance similar to those of RuO_2/Ti with lower operating potentials (Figure S13). Meanwhile, the PdO/Ti anode is continuously oxidized during the reaction, resulting in a continuous increase of the operating potentials (Figure S14). Moreover, the feasibility of halogen-mediated electrochemical epoxidation to different substrates was explored using butylene as the reactant. The results indicated that both Br- and Cl-mediated systems can epoxidize butylene to produce butylene oxide (BO) (Figure S15). Compared with propylene electro-epoxidation, the FE of BO is reduced by approximately 20% under corresponding operating current densities. Considering that butylene has a higher carbon number than propylene, the decreased activity of butylene compared with propylene may lead to the requirement of higher overpotentials for electro-

https://doi.org/10.1021/acsomega.3c05508
ACS Omega 2023, 8, 46569−46576

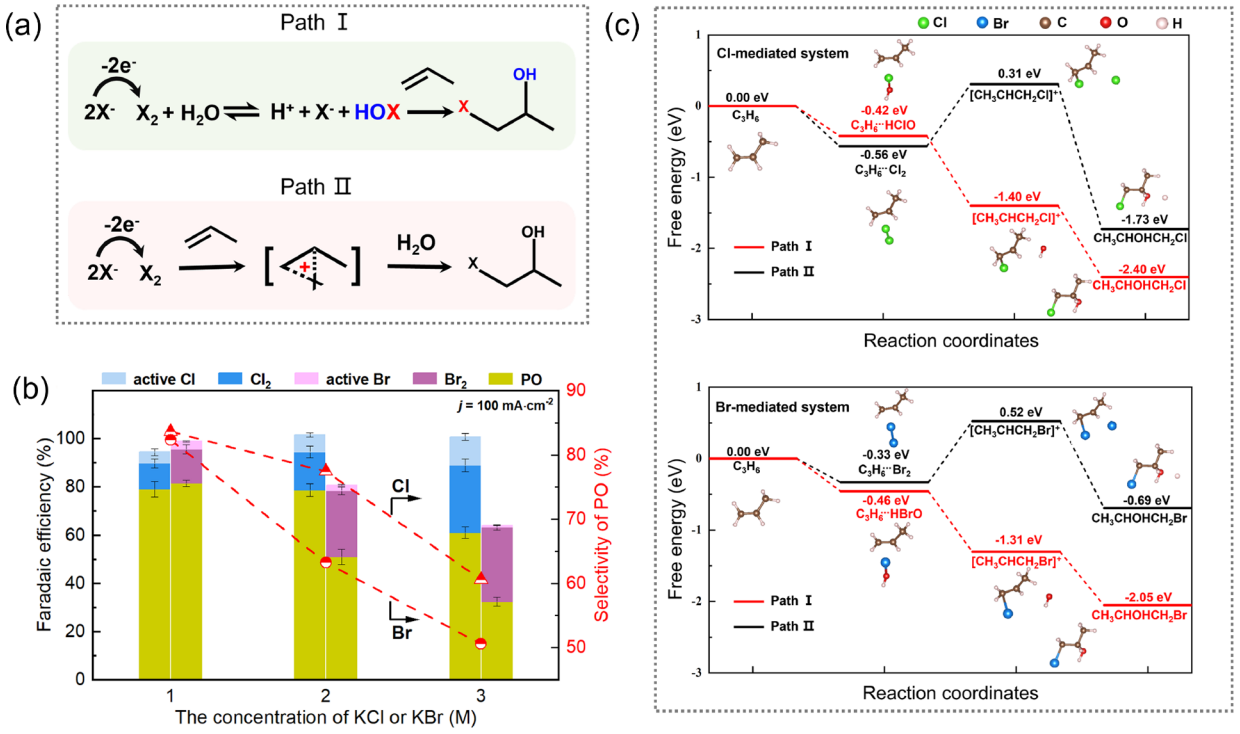

Figure 5. (a) Possible reaction paths for PO electro-epoxidation. (b) Product distribution with varied halogen concentrations. The error bars correspond to the standard deviation of three independent measurements. (c) DFT calculation of the free energy for the intermediates involved in electrophilic attacks.

epoxidation, causing the rise of the OER activity, ultimately resulting in the decrease of the FE for epoxide products (Figure S16).

3.3. Investigation into Reaction Intermediate Species. It is widely debated whether the intermediate species for halogen-mediated olefin epoxidation is a hypochlorous acid molecule or an elemental halogen.[24−26] As shown in Figure 5a, there are mainly two possible paths for the asymmetric addition to the double bond of propylene in the halogen-mediated epoxidation process. The hypochlorous acid-mediated pathway (path I) is functioning via first generating a halogen and then disproportionating it to obtain hypohalous acid. Finally, hypohalous acid is asymmetrically added to the double bond of propylene to form haloalcohol intermediates. Since the process of disproportionation to generate hypohalous acid will generate halide ions at the same time, the amount of hypohalous acid will be sensitive to the concentration of halogen ions (X^-). As the concentration of X^- increases, the equilibrium of the X_2 disproportionation reaction will be reversed, resulting in the precipitation of more halogens instead of generating PO through hypochlorous/hypobromous acid. In contrast, the elemental halogen-mediated pathway (path II) suggested that halonium ions obtained by electrophilic attack of elemental halogens on the double bond would react with H_2O to obtain haloalcohol, which would not be significantly affected by the concentration of X^- in the system. Therefore, we altered the concentration of halide ions in both systems to explore the relationship between the PER performance and the concentration of halide ions in the system.

As a result, the product distributions in systems with different X^- concentrations showed obvious differences (Figure 5b). For instance, when the Br^- concentration increases from 1 to 3 M, the FE_{PO} decreased significantly in the Br-mediated system from 81 to 32%, while the Faradaic efficiency of Br_2 increased from 14 to 31%. A similar trend was also obtained for the Cl-mediated system. Whether it is a Cl- or Br-mediated system, the selectivity of PO showed a consistent downward trend with the increase of the concentration of X^- from 1 to 3 M (79−61% in KCl while 82−32% in KBr), which indicates that the hypochlorous/hypobromous acid should be the key intermediate species rather than the halogen.

DFT calculation further investigated the key intermediate species of the reaction (Figure 5c). For the situation that an elemental halogen as an active species attacks propylene to form halonium ion (path II), a halonium ion intermediate was proposed to be an intermediate species in the electrophilic addition process to alkenes.[27,28] The intermediate species attacks the double bond to obtain the halonium ion intermediate, and then, the hydroxyl group is added to the middle carbon atom through nucleophilic attack. The whole process obeyed Markovnikov rules where electrophilic groups will preferentially combine with edge carbons and nucleophilic groups will preferentially combine with intermediate carbons or carbons containing less hydrogen.[29] However, such a reaction path requires a higher energy barrier, which means that the reaction is more difficult to occur. In contrast, when hypobromous acid and hypochlorous acid are used as media (path I), the formation of halide ion intermediates and the corresponding free energy changes of the nucleophilic addition of hydroxyl groups are all less than zero (Figure 5c), which means that the reaction can proceed spontaneously thermodynamically. These DFT results are consistent with the experimental results, further confirming that hypochlorous and hypobromous acids are more likely to be the key

https://doi.org/10.1021/acsomega.3c05508
ACS Omega 2023, 8, 46569−46576

mediators than an elemental halogen in the process of propylene epoxidation.

4. CONCLUSIONS

In this work, halides were used as electrolytes and oxidation mediators for PO production with a RuO_2/Ti anode driven by electricity. The redox cycle of the Cl and Br on RuO_2/Ti could intervene in the epoxidation of propylene to produce PO with the FEs exceeding 80% at the current density of 100 mA·cm^{-2}. Moreover, a 90% PO FE was achieved at a much lower potential of ≤1.5 V in a Br-mediated system. Furthermore, the hypohalous acid molecules were demonstrated to be the reagent for electrophilic attack on the double bond of propylene rather than the elemental halogen. This work provided an alternative to the traditional chlorohydrin route of PO production, bringing the possibility to couple clean electricity and cathode reactions with high value-added products.

■ ASSOCIATED CONTENT

Supporting Information

The Supporting Information is available free of charge at https://pubs.acs.org/doi/10.1021/acsomega.3c05508.

Materials preparation, product quantifications, electrochemical measurements, and structural characterizations (PDF)

■ AUTHOR INFORMATION

Corresponding Authors

Xiao Dong − *Low-Carbon Conversion Science and Engineering Center, Shanghai Advanced Research Institute, Chinese Academy of Sciences, Shanghai 201210, P.R. China*; Email: dongx@sari.ac.cn

Wei Wei − *Low-Carbon Conversion Science and Engineering Center, Shanghai Advanced Research Institute, Chinese Academy of Sciences, Shanghai 201210, P.R. China; University of the Chinese Academy of Sciences, Beijing 100049, P.R. China; School of Physical Science and Technology, ShanghaiTech University, Shanghai 201203, P.R. China*; orcid.org/0000-0003-0043-1583; Email: weiwei@sari.ac.cn

Wei Chen − *Low-Carbon Conversion Science and Engineering Center, Shanghai Advanced Research Institute, Chinese Academy of Sciences, Shanghai 201210, P.R. China; University of the Chinese Academy of Sciences, Beijing 100049, P.R. China*; orcid.org/0000-0003-3122-2952; Email: chenw@sari.ac.cn

Authors

Jiangjiang Wang − *Low-Carbon Conversion Science and Engineering Center, Shanghai Advanced Research Institute, Chinese Academy of Sciences, Shanghai 201210, P.R. China; University of the Chinese Academy of Sciences, Beijing 100049, P.R. China*

Gangfeng Wu − *Low-Carbon Conversion Science and Engineering Center, Shanghai Advanced Research Institute, Chinese Academy of Sciences, Shanghai 201210, P.R. China; University of the Chinese Academy of Sciences, Beijing 100049, P.R. China*

Guanghui Feng − *Low-Carbon Conversion Science and Engineering Center, Shanghai Advanced Research Institute, Chinese Academy of Sciences, Shanghai 201210, P.R. China; University of the Chinese Academy of Sciences, Beijing 100049, P.R. China*

Guihua Li − *Low-Carbon Conversion Science and Engineering Center, Shanghai Advanced Research Institute, Chinese Academy of Sciences, Shanghai 201210, P.R. China; University of the Chinese Academy of Sciences, Beijing 100049, P.R. China*

Yiheng Wei − *Low-Carbon Conversion Science and Engineering Center, Shanghai Advanced Research Institute, Chinese Academy of Sciences, Shanghai 201210, P.R. China; University of the Chinese Academy of Sciences, Beijing 100049, P.R. China*

Shoujie Li − *Low-Carbon Conversion Science and Engineering Center, Shanghai Advanced Research Institute, Chinese Academy of Sciences, Shanghai 201210, P.R. China*

Jianing Mao − *Low-Carbon Conversion Science and Engineering Center, Shanghai Advanced Research Institute, Chinese Academy of Sciences, Shanghai 201210, P.R. China; University of the Chinese Academy of Sciences, Beijing 100049, P.R. China*

Xiaohu Liu − *Low-Carbon Conversion Science and Engineering Center, Shanghai Advanced Research Institute, Chinese Academy of Sciences, Shanghai 201210, P.R. China; School of Physical Science and Technology, ShanghaiTech University, Shanghai 201203, P.R. China*

Aohui Chen − *Low-Carbon Conversion Science and Engineering Center, Shanghai Advanced Research Institute, Chinese Academy of Sciences, Shanghai 201210, P.R. China; School of Physical Science and Technology, ShanghaiTech University, Shanghai 201203, P.R. China*

Yanfang Song − *Low-Carbon Conversion Science and Engineering Center, Shanghai Advanced Research Institute, Chinese Academy of Sciences, Shanghai 201210, P.R. China*; orcid.org/0000-0002-0392-1441

Complete contact information is available at: https://pubs.acs.org/10.1021/acsomega.3c05508

Author Contributions

The manuscript was written through contributions of all authors. All authors have given approval to the final version of the manuscript.

Notes

The authors declare no competing financial interest.

■ ACKNOWLEDGMENTS

This work was financially supported by the Ministry of Science and Technology of China (National Key R&D Program of China, 2022YFA1504604); the Strategic Priority Research Program of the Chinese Academy of Sciences, "Transformational Technologies for Clean Energy and Demonstration" (XDA 21000000); the Major Project of the Science and Technology department of Inner Mongolia (2021ZD0020); the Youth Innovation Promotion Association of the Chinese Academy of Sciences (E224301401); the Shanghai Sailing Program (23YF1453300 and 18YF1425700); the Shanghai Pujiang Program (20PJ1415200); the Outstanding Young Talent Project of Shanghai Advanced Research Institute, the Chinese Academy of Sciences (E254991ZZ1); and the Foundation of Key Laboratory of Low-Carbon Conversion Science & Engineering, Shanghai Advanced Research Institute, Chinese Academy of Sciences (KLLCCSE-202207Z, SARI, CAS).

https://doi.org/10.1021/acsomega.3c05508
ACS Omega 2023, 8, 46569−46576

REFERENCES

(1) Nijhuis, T. A.; Makkee, M.; Moulijn, J. A.; Weckhuysen, B. M. The production of propene oxide: Catalytic processes and recent developments. *Ind. Eng. Chem. Res.* **2006**, *45* (10), 3447−3459.

(2) Karmadonova, I. E.; Zudin, V. N.; Kuznetsova, N. I.; Kuzhetsova, L. I.; Bal'zhinimaev, B. S. Preparation of Ethylbenzene and Isopropylbenzene Hydroperoxides in the N-Hydroxyphthalimide-Fe (III) Homogeneous Catalytic System and Use of Solutions in the Epoxidation of Olefins. *Catal. Ind.* **2020**, *12* (3), 216−225.

(3) Buijink, J. K. F.; van Vlaanderen, J.; Crocker, A.; Niele, E. M. Propylene epoxidation over titanium-on-silica catalyst - the heart of the SMPO process. *Catal. Today* **2004**, *93* (5), 199−204.

(4) Zuwei, X.; Ning, Z.; Yu, S.; Kunlan, L. Reaction-controlled phase-transfer catalysis for propylene epoxidation to propylene oxide. *Science* **2001**, *292* (5519), 1139−1141.

(5) Signorile, M.; Braglia, L.; Crocella, V.; Torelli, P.; Groppo, E.; Ricchiardi, G.; Bordiga, S.; Bonino, F. Titanium Defective Sites in TS-1: Structural Insights by Combining Spectroscopy and Simulation. *Angew. Chem.-Int. Ed.* **2020**, *59* (41), 18145−18150.

(6) Gordon, C. P.; Engler, H.; Tragl, A. S.; Plodinec, M.; Lunkenbein, T.; Berkessel, A.; Teles, J. H.; Parvulescu, A. N.; Coperet, C. Efficient epoxidation over dinuclear sites in titanium silicalite-1. *Nature* **2020**, *586* (7831), 708.

(7) Li, Y.; Ozden, A.; Leow, W. R.; Ou, P.; Huang, J. E.; Wang, Y.; Bertens, K.; Xu, Y.; Liu, Y.; Roy, C.; Jiang, H.; Sinton, D.; Li, C.; Sargent, E. H. Redox-mediated electrosynthesis of ethylene oxide from CO_2 and water. *Nat. Catal.* **2022**, *5* (3), 185−192.

(8) Ke, J.; Zhao, J.; Chi, M.; Wang, M.; Kong, X.; Chang, Q.; Zhou, W.; Long, C.; Zeng, J.; Geng, Z. Facet-dependent electrooxidation of propylene into propylene oxide over Ag_3PO_4 crystals. *Nat. Commun.* **2022**, *13* (1), 932.

(9) Xu, R.; Huang, H.; Wang, W.; Ding, L.; Lin, Q.; Li, J.; Zhang, Y.; Han, Y.; Wang, J.; Lu, X. Direct conversion of water to hydrogen peroxide on single electrode towards partial oxidation of propylene. *Chem. Eng. J.* **2023**, *461*, No. 141748, DOI: 10.1016/j.cej.2023.141748.

(10) Leow, W. R.; Lum, Y.; Ozden, A.; Wang, Y.; Nam, D.-H.; Chen, B.; Wicks, J.; Zhuang, T. T.; Li, F.; Sinton, D.; Sargent, E. H. Chloride-mediated selective electrosynthesis of ethylene and propylene oxides at high current density. *Science* **2020**, *368* (6496), 1228.

(11) Zhang, Y.; Iqbal, A.; Zai, J.; Li, W.; Guo, H.; Meng, X.; Li, W.; Islam, I. U.; Xin, Z.; Qian, X. Balanced cathodic debromination and hydrogen evolution reactions endow highly selective epoxidation of styrene. *Composites Part B* **2022**, *246*, No. 110281.

(12) Chung, M.; Jin, K.; Zeng, J. S.; Manthiram, K. Mechanism of Chlorine-Mediated Electrochemical Ethylene Oxidation in Saline Water. *ACS Catal.* **2020**, *10* (23), 14015−14023.

(13) Li, W.; Chen, L.; Qiu, M.; Li, W.; Zhang, Y.; Zhu, Y.; Li, J.; Chen, X. Highly Efficient Epoxidation of Propylene with In Situ-Generated H2O2 over a Hierarchical TS-1 Zeolite-Supported Non-Noble Nickel Catalyst. *ACS Catal.* **2023**, *13* (15), 10487−10499.

(14) Feng, X.; Duan, X.; Yang, J.; Qian, G.; Zhou, X.; Chen, D.; Yuan, W. Au/uncalcined TS-1 catalysts for direct propene epoxidation with H2 and O2: Effects of Si/Ti molar ratio and Au loading. *Chem. Eng. J.* **2015**, *278*, 234−239.

(15) Exner, K. S.; Anton, J.; Jacob, T.; Over, H. Full Kinetics from First Principles of the Chlorine Evolution Reaction over a RuO_2 (110) Model Electrode. *Angew. Chem., Int. Ed.* **2016**, *55* (26), 7501−7504.

(16) Kresse, G.; Furthmuller, J. Efficiency of ab-initio total energy calculations for metals and semiconductors using a plane-wave basis set. *Comput. Mater. Sci.* **1996**, *6* (1), 15−50.

(17) Perdew, J. P.; Burke, K.; Ernzerhof, M. Generalized Gradient Approximation Made Simple. *Phys. Rev. Lett.* **1996**, *77* (18), 3865−3868.

(18) Grimme, S.; Ehrlich, S.; Goerigk, L. Effect of the damping function in dispersion corrected density functional theory. *J. Comput. Chem.* **2011**, *32* (7), 1456−1465.

(19) Mathew, K.; Sundararaman, R.; Letchworth-Weaver, K.; Arias, T. A.; Hennig, R. G. Implicit solvation model for density-functional study of nanocrystal surfaces and reaction pathways. *J. Chem. Phys.* **2014**, *140* (8), 8.

(20) Bertrand, X.; Chabaud, L.; Paquin, J. F. Hydrofluorination of Alkenes: A Review. *Chem-Asian. J.* **2021**, *16* (6), 563−574.

(21) Angulo, A.; van der Linde, P.; Gardeniers, H.; Modestino, M.; Rivas, D. F. Influence of Bubbles on the Energy Conversion Efficiency of Electrochemical Reactors. *Joule* **2020**, *4* (3), 555−579.

(22) Zhao, X.; Ren, H.; Luo, L. Gas Bubbles in Electrochemical Gas Evolution Reactions. *Langmuir* **2019**, *35* (16), 5392−5408.

(23) Karlsson, R. K. B.; Cornell, A. Selectivity between Oxygen and Chlorine Evolution in the Chlor-Alkali and Chlorate Processes. *Chem. Rev.* **2016**, *116* (5), 2982−3028.

(24) Liu, X.; Chen, Z.; Xu, S.; Liu, G.; Zhu, Y.; Yu, X.; Sun, L.; Li, F. Bromide-Mediated Photoelectrochemical Epoxidation of Alkenes Using Water as an Oxygen Source with Conversion Efficiency and Selectivity up to 100%. *J. Am. Chem. Soc.* **2022**, *144* (43), 19770−19777.

(25) Ha, H.; Jin, K.; Park, S.; Lee, K. G.; Cho, K. H.; Seo, H.; Ahn, H. Y.; Lee, Y. H.; Nam, K. T. Highly selective active chlorine generation electrocatalyzed by Co_3O_4 nanoparticles: Mechanistic investigation through in situ electrokinetic and spectroscopic analyses. *J. Phys Chem. Lett.* **2019**, *10*, 1226.

(26) Zhao, Y.; Duan, M.; Deng, C.; Yang, J.; Yang, S.; Zhang, Y.; Sheng, H.; Li, Y.; Chen, C.; Zhao, J. Br^-/BrO^--mediated highly efficient photoelectrochemical epoxidation of alkenes on alpha-Fe_2O_3. *Nat. Commun.* **2023**, *14* (1), 1943.

(27) Alkire, R.; Köhler, J. Indirect electrochemical epoxidation of hexene in a liquid-liquid electrolyte. *J. Appl. Electrochem.* **1988**, *18* (3), 405−409.

(28) Torii, S.; Uneyama, K.; Tanaka, H.; Yamanaka, T.; Yasuda, T.; Ono, M.; Kohmoto, Y. Efficient conversion of olefins into epoxides, bromohydrins, and dibromides with sodium bromide in water-organic solvent electrolysis systems. *Org. Chem.* **1981**, *46* (16), 3312−3315.

(29) Beletskaya, I. P.; Nenajdenko, V. G. Towards the 150th Anniversary of the Markovnikov Rule. *Angew. Chem., Int. Ed. Engl.* **2019**, *58* (15), 4778−4789.

https://doi.org/10.1021/acsomega.3c05508
ACS Omega 2023, 8, 46569−46576